PERGAMON

International Journal of Heat and Mass Transfer 42 (1999) 789–802

International Journal of HEAT and MASS TRANSFER

Heat transfer on a film-cooled rotating blade using different turbulence models

Vijay K. Garg*

AYT Corporation, NASA Lewis Research Center, 21000 Brookpark Road, Mail Stop 5-11, Cleveland, OH 44135, U.S.A.

Received 26 November 1997; in final form 15 July 1998

Abstract

A three-dimensional Navier–Stokes code has been used to compute the heat transfer coefficient on a film-cooled, rotating turbine blade. The blade chosen is the ACE rotor with five rows containing 93 film cooling holes covering the entire span. This is the only film-cooled rotating blade over which experimental data is available for comparison. Over 2.278 million grid points are used to compute the flow over the blade including the tip clearance region, using Wilcox's k–ω model, Coakley's q–ω model, and the zero-equation Baldwin–Lomax (B–L) model. A reasonably good comparison with the experimental data is obtained on the suction surface for all the turbulence models. At the leading edge, the B–L model yields a better comparison than the two-equation models. On the pressure surface, however, the comparison between the experimental data and the prediction from the k–ω model is much better than from the other two models. Overall, the k–ω model provides the best comparison with the experimental data. However, the two-equation models require at least 40% more computational resources than the B–L model.

Nomenclature

B_p blowing parameter $[=(\rho_c V_c)/\{\rho_o (RT_0)^{1/2}\}]$
c_a axial chord of the blade
C_D discharge coefficient for the hole
C_p specific heat at constant pressure
d coolant hole diameter
e total energy
H specific total enthalpy
J Jacobian of the coordinate transformation
k turbulence kinetic energy
k_w gas thermal conductivity at the blade temperature
l turbulence length scale
M Mach number
Nu Nusselt number based on c_a, $(T_{o,rel}-T_w)$ and k_w
p pressure
Pr Prandtl number
q square root of turbulence kinetic energy
r radial coordinate
R gas constant
Re Reynolds number
s distance from the leading edge along the pressure or suction surface
S $=s/s_m$ on suction surface, and $=-s/s_m$ on pressure surface
T temperature
Tu turbulence intensity
u, v, w absolute velocity components in the Cartesian coordinate system
U, V, W contravariant velocity components
V_c average coolant velocity at the hole exit
(x, y, z) Cartesian coordinate system with origin at the geometric stagnation point, and z coordinate along the span
y^+ distance in wall coordinates off the blade surface
z^+ distance in wall coordinates off the hub or off the shroud.

Greek symbols

γ ratio of specific heats
Δy distance (from the wall) of the first point off the wall
ε turbulence dissipation rate
μ viscosity
ν kinematic viscosity
ρ density
ω specific turbulence dissipation rate $(=\varepsilon/k)$
(ξ, η, ζ) curvilinear coordinate system with ξ wrapping

* Corresponding author. E-mail: vijay.garg@lerc.nasa.gov

0017–9310/98/$—see front matter
PII: S0017–9310(98)00229–4

around the blade, η running blade-to-blade, and ζ running spanwise
Ξ vorticity
Ω rotational speed of the blade.

Subscripts
c for coolant (average value)
ef effective value
ex value at exit of rotor
in value at inlet
,*i* derivative with respect to *i*-direction coordinate.
l laminar
m maximum value
o stagnation value
rel value relative to the rotor
T turbulent value
w value at wall

1. Introduction

The search for better performance of gas turbine engines has led to higher turbine inlet temperatures. Modern gas turbine engines are designed to operate at inlet temperatures of 1800–2000 K, which are far beyond the allowable metal temperatures. Under these conditions, the turbine blades need to be cooled in order to ensure a reasonable lifetime. This calls for an efficient cooling system. Discrete jet film cooling is one of the techniques used to protect the blades and endwalls that are thermally exposed. Since the injected cooler air is bled directly from the compressor before it passes through the combustion chamber, the best compromise between admissible metal temperature and aerodynamic efficiency becomes a major objective in cooled turbine blade design.

A considerable effort has been devoted to understanding the coolant film behavior and its interaction with the mainstream flow. The film cooling performance is influenced by the wall curvature, three-dimensional external flow structure, free-stream turbulence, compressibility, flow unsteadiness, the hole size, shape and location, and the angle of injection. Many studies on film cooling have been confined to simple geometries, for example, two-dimensional flat and curved plates in steady, incompressible flow. An excellent survey of the work up to 1971 has been provided by Goldstein [1]. While several further studies in this field have been summarized by Garg and Gaugler [2–4], some relevant ones are discussed here.

Among the approaches to the prediction of film cooling performance, one is to model the penetration, spreading and entrainment of the main flow by the coolant jets from the discrete holes. These interaction models have been incorporated into boundary layer codes [5–7] or into two-dimensional Navier–Stokes code [8]. In another approach, Garg and Gaugler [2–4, 9, 10] used a three-dimensional Navier–Stokes code with surface injection to model the film cooling performance around the C3X vane, and the VKI and ACE rotor cascades, while Garg [11], and Garg and Abhari [12] analyzed film-cooled rotating blades, specifically the UTRC rotor and the ACE rotor. In this approach, similar to the present technique, the film holes are modeled by adding, as a boundary condition, the appropriate amount of mass, momentum and energy flux distribution at the discrete location of the film holes. They compared the predictions to the experimental measurements on these cascades and rotating blades, and found a fairly good agreement using the B–L model. The computational results clearly illustrated the three-dimensionality of the flow in the near hole region. Recently, Garg and Ameri [13] compared the heat transfer coefficient on the C3X vane and VKI rotor using the B–L and three two-equation turbulence models with the experimental data.

Choi [14] also used a three-dimensional code to predict the flow and the surface heat transfer around a section of the ACE turbine blade. The computational grid was extended into the film holes to model the elliptic nature of the flow at the film hole exit plane. In order to minimize the size of the computational grid and the associated computational resource requirements, Choi only modeled a section of the blade which in the span-wise direction covered one half of a film hole pitch with span-wise periodic boundary conditions. Such a reduction in computational span is possible, however, for a linear cascade only, and was also used by Garg and Gaugler [2–4, 9, 10], and by Garg and Ameri [13]. For a rotating blade, the entire span needs to be discretized in order to model correctly the rotational body forces.

Only three experimental measurements of film cooling on rotating turbine blades are available [15–17]. All three studies concluded that film cooling on the suction surface provides good surface protection, while on the pressure surface the results are mixed. The measurement database of Abhari [16] provides the experimental results for the present numerical study.

The goal of the present study is to predict the heat transfer on a rotating film-cooled blade using different turbulence models, and compare the predictions with the experimental data of Abhari [16] on the ACE turbine rotor. A number of operating conditions with film cooling were simulated using the B–L, k–ω and q–ω turbulence models, and the predicted results compared to the experimental data. These comparisons combined with observations from the surface heat loads on the blade are used to evaluate the various turbulence models for the film cooling of rotor blades.

2. Analysis

The three-dimensional Navier–Stokes code of Arnone [18] for the analysis of turbomachinery flows was modi-

fied by Garg and Gaugler [3] to include film cooling effects. Briefly, the code is an explicit, multigrid, cell-centered, finite volume code. The Navier–Stokes equations in a rotating Cartesian coordinate system are mapped onto a general body-fitted (ξ, η, ζ) coordinate system using standard techniques. The governing equations are:

$$\partial_t(J^{-1}Q)+\partial_\xi E+\partial_\eta F+\partial_\zeta G=\partial_\xi E_V+\partial_\eta F_V+\partial_\zeta G_V+I \tag{1}$$

where

$$Q=\begin{bmatrix}\rho\\ \rho u\\ \rho v\\ \rho w\\ \rho\theta\end{bmatrix},\quad E=J^{-1}\begin{bmatrix}\rho U\\ \rho uU+\xi_x p\\ \rho vU+\xi_y p\\ \rho wU+\xi_z p\\ \rho HU-\xi_t p\end{bmatrix},$$

$$F=J^{-1}\begin{bmatrix}\rho V\\ \rho uV+\eta_x p\\ \rho vV+\eta_y p\\ \rho wV+\eta_z p\\ \rho HV-\eta_t p\end{bmatrix},\quad G=J^{-1}\begin{bmatrix}\rho W\\ \rho uW+\zeta_x p\\ \rho vW+\zeta_y p\\ \rho wW+\zeta_z p\\ \rho HW-\zeta_t p\end{bmatrix}$$

$$I=\Omega[0\quad 0\quad \rho w\quad -\rho v\quad 0]^T. \tag{2}$$

The contravariant velocity components in equation (2) are

$$U=\xi_t+\xi_x u+\xi_y v+\xi_z w,\quad V=\eta_t+\eta_x u+\eta_y v+\eta_z w,$$
$$W=\zeta_t+\zeta_x u+\zeta_y v+\zeta_z w \tag{3}$$

and the metric terms are defined by

$$\begin{bmatrix}\xi_x & \eta_x & \zeta_x\\ \xi_y & \eta_y & \zeta_y\\ \xi_z & \eta_z & \zeta_z\end{bmatrix}=J\begin{bmatrix}y_\eta z_\zeta-y_\zeta z_\eta & y_\zeta z_\xi-y_\xi z_\zeta & y_\xi z_\eta-y_\eta z_\xi\\ x_\zeta z_\eta-x_\eta z_\zeta & x_\xi z_\zeta-x_\zeta z_\xi & x_\eta z_\xi-x_\xi z_\eta\\ x_\eta y_\zeta-x_\zeta y_\eta & x_\zeta y_\xi-x_\xi y_\zeta & x_\xi y_\eta-x_\eta y_\xi\end{bmatrix}$$

$$\xi_t=-x_t\xi_x-y_t\xi_y-z_t\xi_z,\quad \eta_t=-x_t\eta_x-y_t\eta_y-z_t\eta_z$$
$$\zeta_t=-x_t\zeta_x-y_t\zeta_y-z_t\zeta_z,\quad x_t=0,\quad y_t=-\Omega z,\quad z_t=\Omega y \tag{4}$$

where the Jacobian is given by

$$J=(x_\xi y_\eta z_\zeta+x_\zeta y_\xi z_\eta+x_\eta y_\zeta z_\xi-x_\xi y_\zeta z_\eta-x_\eta y_\xi z_\zeta-x_\zeta y_\eta z_\xi)^{-1}. \tag{5}$$

The viscous flux term, E_v, is given by

$$E_V=J^{-1}\begin{bmatrix}0\\ \xi_x\tau_{xx}+\xi_y\tau_{xy}+\xi_z\tau_{xz}\\ \xi_x\tau_{yx}+\xi_y\tau_{yy}+\xi_z\tau_{yz}\\ \xi_x\tau_{zx}+\xi_y\tau_{zy}+\xi_z\tau_{zz}\\ \xi_x\beta_x+\xi_y\beta_y+\xi_z\beta_z\end{bmatrix} \tag{6}$$

with F_V and G_V obtained from E_V by replacing ξ by η and ζ, respectively, and where

$$\tau_{xx}=2\mu u_x+\lambda(u_x+v_y+w_z),$$
$$\tau_{yy}=2\mu v_y+\lambda(u_x+v_y+w_z),$$
$$\tau_{zz}=2\mu w_z+\lambda(u_x+v_y+w_z),$$
$$\tau_{xy}=\tau_{yx}=\mu(u_y+v_x),\quad \tau_{xz}=\tau_{zx}=\mu(u_z+w_x),$$
$$\tau_{yz}=\tau_{zy}=\mu(v_z+w_y),\quad \beta_x=u\tau_{xx}+v\tau_{xy}+w\tau_{xz}+kT_x,$$
$$\beta_y=u\tau_{yx}+v\tau_{yy}+w\tau_{yz}+kT_y,$$
$$\beta_z=u\tau_{zx}+v\tau_{zy}+w\tau_{zz}+kT_z. \tag{7}$$

The Cartesian derivatives in equation (7) are expressed, using the chain rule, as

$$u_x=\xi_x u_\xi+\eta_x u_\eta+\zeta_x u_\zeta. \tag{8}$$

According to Stokes' hypothesis, λ is taken to be $-2\mu/3$.

The equations are non-dimensionalized by the inlet total density ρ_o, the blade axial chord as the characteristic length, and $(RT_o)^{1/2}$ as the characteristic velocity. It is assumed that the effective viscosity for turbulent flows can be written as

$$\mu_{ef}=\mu_l+\mu_T \tag{9}$$

where the laminar viscosity μ_l is calculated using Sutherland's law [19]. The turbulent viscosity μ_T is computed using the two-equation models as described below. Also, the effective thermal conductivity is taken to be

$$k_{ef}=C_p[(\mu/Pr)_l+(\mu/Pr)_T]. \tag{10}$$

The multistage Runge–Kutta scheme developed by Jameson et al. [20] is used to advance the flow solution in time from an initial guess to the steady state. To accelerate convergence the code employs the Full Approximation Storage (FAS) multigrid method originally devised by Brandt [21] and Jameson [22]. Variable coefficient implicit smoothing of the residuals is performed to improve further the rate of convergence. A three-dimensional extension of eigenvalue scaling of the artificial dissipation terms, first devised by Martinelli [23], was adopted to prevent odd–even decoupling and to capture shocks. A spatially varying time step along with a Courant–Friedrichs–Levy (CFL) number of four was used to speed convergence to the steady state.

2.1. Turbulence models

Turbulence was modeled using two low-Reynolds number two-equation models. Transition to turbulence is automatically mimicked by such models. Wilcox's k–ω and Coakley's q–ω models were selected for comparison with the experimental data, and with the algebraic mixing length turbulence model of Baldwin and Lomax [24]. The general formulation for the two-equation models can be written as

$$(\rho s_i)_{,t}+(\rho s_i u_j+q_{ij})_{,j}=H_i$$

$$q_{ij} = -(\mu+\mu_T/Pr_i)s_{i,j}, \quad i = 1,2. \quad (11)$$

For Coakley's q–ω model [25], the variables s_1 and s_2 are

$$s_1 = q, \quad s_2 = \omega, \quad \mu_T = C_\mu D\rho q^2/\omega. \quad (12)$$

The source terms in the model equations are

$$H_q = \tfrac{1}{2}[C_\mu DS/\omega - \tfrac{2}{3}\Im - \omega]\rho q$$

$$H_\omega = [C_1(C_\mu S/\omega - 2/3\Im) - C_2\omega]\rho\omega. \quad (13)$$

The strain rate invariant S, and the divergence of the velocity $\Im$, appearing in equation (13) are

$$S = (u_{i,j}+u_{j,i}-\tfrac{2}{3}\delta_{ij}u_{k,k})u_{i,j}, \quad \Im = u_{k,k}. \quad (14)$$

Following Menter [26], however, it was found that taking S to be the square of vorticity yielded better convergence characteristics and surface heat transfer results. D is a damping function defined as

$$D = 1-\exp(-\alpha R), \quad R = qy/v$$

and

$$Pr_q = 1.0, \quad Pr_\omega = 1.3, \quad C_\mu = 0.09$$

$$C_1 = 0.405D+0.045, \quad C_2 = 0.92, \quad \alpha = 0.0065.$$

For Wilcox's k–ω model [27], the variables s_1 and s_2 are

$$s_1 = k, \quad s_2 = \omega, \quad \mu_T = \alpha^*\rho k/\omega.$$

With Menter's modifications [26], the source terms in the model equations are

$$H_k = \mu_T\Xi^2 - \tfrac{2}{3}\Im\rho k - \beta^*\rho k\omega$$

$$H_\omega = \alpha(\mu_T\Xi^2/k - \tfrac{2}{3}\Im\rho)\omega - \beta\rho\omega^2 \quad (15)$$

where Ξ is the vorticity. The coefficients appearing in the model are

$$Pr_k = Pr_\omega = 2, \quad \beta = 3/40,$$

$$\beta^* = 0.09F_\beta, \quad \alpha = (5/9)(F_\alpha/F_\mu)$$

$$F_\beta = \frac{5/18+(Re_T/R_\beta)^4}{1+(Re_T/R_\beta)^4}, \quad F_\alpha = \frac{\alpha_0+Re_T/R_\omega}{1+Re_T/R_\omega}$$

$$F_\mu = \alpha^* = \frac{\alpha_0^*+Re_T/R_k}{1+Re_T/R_k}, \quad Re_T = \frac{\rho k}{\mu\omega}$$

$$\alpha_0 = 0.1, \quad \alpha_0^* = 0.025, \quad R_\beta = 8,$$

$$R_\omega = 2.7, \quad R_k = 6. \quad (16)$$

Use of y^+ in damping functions is proper for attached wall flows; it is not very meaningful once the flow separates. The k–ω model obviates this problem by dispensing with the use of y^+, calculation of which can be tedious for a three-dimensional problem specially when using a multi-block code.

The turbulence model equations were incorporated into the code and solved explicitly along with the flow equations, following Ameri and Arnone [28, 29]. No fourth-order dissipation terms were needed for the turbulence model equations. Variable coefficient implicit residual smoothing was adapted to the model equations as well by setting up the coefficients using the eigenvalues of the model equations. This along with proper linearization of the source terms in the model equations and implicit solution for k or q and ω allowed the use of CFL = 2 for the turbulence model equations while CFL = 4 for the flow equations.

2.2. Boundary conditions

At the inflow boundary, the total temperature, total pressure, whirl and meridional flow angle are specified, and the upstream-running Riemann invariant based on the total absolute velocity is calculated at the first interior point and extrapolated to the inlet. The velocity components are then decoupled algebraically, and the density is found from total temperature, total pressure and total velocity using an isentropic relation. For the turbulence model, the value of k or q and ω is specified using the experimental conditions, namely

$$q = k^{1/2} = \sqrt{1.5}u_{in}Tu_{in}, \quad \omega = q/l = k^{1/2}/l$$

where Tu_{in} is the intensity of turbulence at the inlet (taken to be 0.15 as the NGVs precede the rotor), u_{in} is the inlet velocity, and l is the turbulence length scale representing the size of the energy containing eddies. This length scale is usually not reported as part of the experimental conditions, and needs to be assumed. For the present study, l was assumed to be 5% of the blade axial chord. Garg and Ameri [13] report that using Chien's k–ε model and changing l to 0.01 or 0.25 for the C3X vane resulted in negligible difference in the heat transfer coefficient at the blade surface as compared to that for $l = 0.05$. It is reasonable to assume that similar results would hold for the ACE rotor using the k–ω or q–ω model.

At the exit, the hub static pressure is specified and the density and velocity components are extrapolated from the interior. The local static pressure is found by integrating the axisymmetric radial equilibrium equation. Periodic flow conditions in terms of cylindrical velocity components are set on a dummy grid line outside the boundary. At the solid surfaces (the hub, the shroud and the rotating blade), the no-slip condition is enforced. The boundary conditions for turbulence quantities on the walls are $k = q = 0$. For the q–ω model, $\partial\omega/\partial n = 0$ at the wall, while for the k–ω model,

$$\omega = 100\left.\frac{\partial u}{\partial y}\right|_{wall}$$

for a hydraulically smooth surface. An upper limit is imposed on the value of ω at the wall, as suggested by Menter [26] and found effective by Chima [30],

$$(\omega_{max})_{wall} = \frac{800}{Re}\frac{v}{(\Delta y)^2}.$$

The experimental values for the blade temperature were known at only 25 points on the blade surface, while the computational grid had over 38 000 grid points on the blade surface. Thus, in the absence of a complete

surface temperature map, the blade surface was considered isothermal. The largest experimental variations in the blade surface temperature relative to the mean were as much as 12–20% of the temperature difference, $T_{o,rel} - T_w$, used to compute the Nusselt number. The hub and shroud surfaces were also considered isothermal and assumed to be at the same temperature as the blade. Based upon an estimate obtained from a streamline curvature prediction, the boundary layer thickness on the hub and shroud was taken to be 10 and 15% of span, respectively, for the incoming flow to the rotor. The vena contracta of each hole was accounted for by reducing the actual hole exit area by the values of the estimated discharge coefficient, C_D, reported in Table 1.

The effects of film cooling have been incorporated into the code in the form of appropriate boundary conditions at the hole locations on the blade surface. Each hole exit is represented by several control volumes having a total area equal to the area of the hole exit, and passing the same coolant mass flow, with the discharge coefficient for the hole having been taken into account. Different velocity and temperature profiles for the injected gas can be specified at the hole exit. For the cases reported here, uniform distribution of the coolant velocity (relative to the blade), temperature, turbulence intensity and length scale at the hole exit was specified. We may point out that using the Baldwin–Lomax model, Garg and Abhari [12] report that a polynomial distribution of coolant velocity and temperature at the exit of the double-row of holes on the pressure surface did not produce any appreciable difference in the Nusselt number values on the pressure surface. Turbulence intensity at the hole exit was assumed to be 0.12, while the turbulence length scale at the hole exit was taken to be $0.1d$ in the absence of any experimental data for these quantities. It was found, however, that changing Tu to 0.06 and/or l to $0.5d$ at the hole exit resulted in a negligible change in the heat transfer coefficient at the blade surface, except in the immediate vicinity of the holes.

3. ACE rotor and experimental details

The Rolls–Royce ACE high pressure transonic turbine model was the test object on which film cooling data were taken in the short duration (0.3 s measurement time), blowdown, rotating turbine rig facility at M.I.T. by Abhari [16]. In this facility, it is possible to simulate full engine scale Reynolds number, Mach number, Prandtl number, gas to wall and coolant to mainstream temperature ratios, specific heat ratios and flow geometry while operating under benign operating conditions. A mixture of argon and freon-12 was used for the main flow while a mixture of argon and freon-14 was used as the coolant in order to prevent condensation at the low temperatures and high pressures of the coolant supply system. Values of the gas constant and specific heat ratios for the mainstream and coolant flows are given in Tables 2 and 3.

The ACE turbine geometry and cooling arrangement are shown schematically in Fig. 1. This turbine had a 551.2 mm rotor diameter with 36 nozzle guide vanes (NGVs) and 61 rotor blades. The rotor blades had an axial chord of 26.1 mm, and five film cooling rows containing 93 holes. For the cooled rotor tests, thin walled NGVs were used with slot injection near the pressure surface trailing edge sized to pass the flow of a fully cooled NGV. Three instrumented and six other solid

Table 2
Main flow parameters

Case	p_o [kPa]	T_o [K]	p_{ex} [kPa]	Ω [rpm]	T_w [K]	γ
71	450.0	486.0	117.537	7087	321.3	1.246
72	460.0	490.0	128.683	5610	325.0	1.255
73	351.0	417.0	92.206	6330	310.0	1.276

$R = 125.1\ \mathrm{J\ kg^{-1}\ K^{-1}}$

Table 1
Hole characteristics

	Estimated discharge coefficient, C_D											
	Hub for case			Mid-span for case			Tip for case			Stream-wise angle (deg)	Hole-shape	No of holes
Hole-row	71	72	73	71	72	73	71	72	73			
PS1	0.52	0.63	0.57	0.64	0.66	0.64	0.63	0.67	0.66	60	Cylinder	18
PS21	0.50	0.63	0.62	0.62	0.64	0.64	0.60	0.65	0.65	30	Cylinder	19
PS22	0.56	0.63	0.61	0.62	0.64	0.63	0.64	0.65	0.64	30	Cylinder	18
SS1	0.52	0.37	0.52	0.59	0.45	0.56	0.62	0.56	0.61	30	D-shape	18
SS2	0.48	0.48	0.48	0.39	0.39	0.39	0.46	0.46	0.46	30	Cylinder	20

Hole diameter = 0.5 mm; spanwise pitch = 2 mm; spanwise angle = 90°

Table 3
Coolant flow parameters

Case	γ_c	$T_{o,rel}$ [K]	$p_{o,rel}$ [kPa]		
			Hub	Mid-span	Tip
71	1.406	222.5	241.761	255.238	262.229
72	1.405	224.5	258.683	268.410	275.503
73	1.406	222.9	194.645	204.373	212.276

$R_c = 158.5\ \mathrm{J\ kg^{-1}\ K^{-1}}$

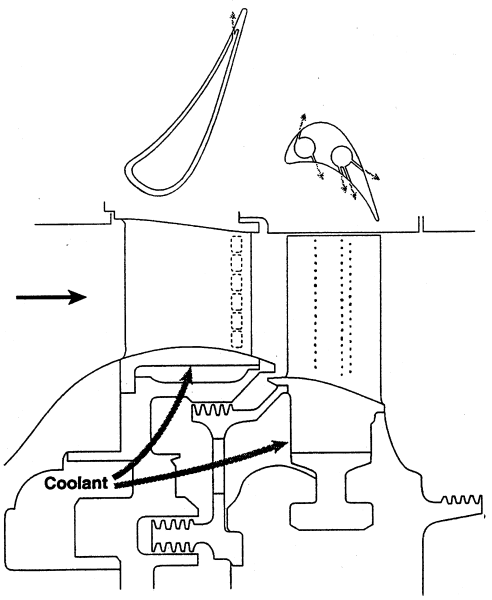

Fig. 1. ACE turbine geometry and cooling arrangement.

aluminum rotor blades were drilled out for two radially positioned coolant supply plenums; the other 52 rotor blades were of steel shell construction. The coolant film hole internal diameter was 0.5 mm, and length to diameter ratio was large (>20) for all holes. All rows had circular exit areas except for the first row (SS1) on the suction surface which was D-shaped. The cooling configuration consisted of: (a) one 30° single row (SS1) of 18 D-shaped holes (fanned at 25° half angle in the spanwise direction with an exit width of 1.25 mm) at about 20% surface length on the suction surface; (b) one 30° single row (SS2) of 20 round holes at about 70% surface length on the suction surface; (c) one 60° single row (PS1) of 18 holes at about 25% surface length on the pressure surface; and (d) one 30° double row of 19 (PS21) and 18 (PS22) staggered holes, with a chordwise spacing of 2 mm, at about 50% surface length on the pressure surface. All holes were drilled at 90° from the radial direction. More details in terms of estimated discharge coefficient for the holes are available in Table 1. Figure 2 shows a small portion of the unfolded part of the blade containing the holes. The ordinate in Fig. 2 denotes the distance along the blade surface in the spanwise direction, while the abscissa denotes the distance, measured from the leading edge, along the blade surface in the streamwise direction, both normalized by the hole diameter, d. The shape and orientation of the hole openings in Fig. 2 is a direct consequence of the angles the holes make with the streamwise direction.

The heat flux from the free-stream to the blade was measured with thin film heat flux gauges distributed about the blade profile. These transducers are 25 μm thick with a rectangular sensing area (1.0×1.3 mm), oriented such that the longest dimension is in the chordwise direction. The coolant hole and heat flux gauge locations are shown in Fig. 3. The top chordwise row will be referred to as the tip location, the middle as mid-span and the bottom as the hub gauges. Note that none of the three rows of gauges is at a fixed radial location. Unfortunately, several of the gauges failed over the course of the testing, especially on the pressure surface. Thus, not all measurement locations yielded data at all test conditions. High frequency response pressure transducers and thermocouples were installed in the NGVs and rotor blades to monitor the conditions in the coolant hole supply plenums. Facility measurements included inlet total temperature and pressure, outlet total pressure, wall static pressures, and rotor speed. More details are available in [16].

4. Computational details

The grid size is non-uniform in all directions so as to pack more grid points within the hole-exits and near the boundary layers on the blade, the hub and the shroud. For computational accuracy, the ratio of two adjacent grid sizes in any direction was kept within 0.76 to 1.3. A periodic C-grid with over 2 278 000 grid points was used. The grid used was $225 \times 45 \times 225$ where the first number represents the number of grid points along the wrap-around direction for the C-grid, the second in the blade-to-blade direction, and the third in the span direction. This grid was arrived at following numerical experimentation with a coarser grid $133 \times 41 \times 113$ that yielded Nusselt number values at the blade surface about 10% different from those presented here. Normal to the blade surface is the dense viscous grid, with $y^+ < 1.0$ for the first point off the blade surface, following Boyle and Giel [31], and Hall et al. [32]. Normal to the hub and shroud also is a dense grid, with $z^+ < 2.5$ for the first point off the hub or off the shroud. Also, the tip clearance region was taken to be 1% of the blade span (static measurement) with 20 grid points within it. The tip clearance

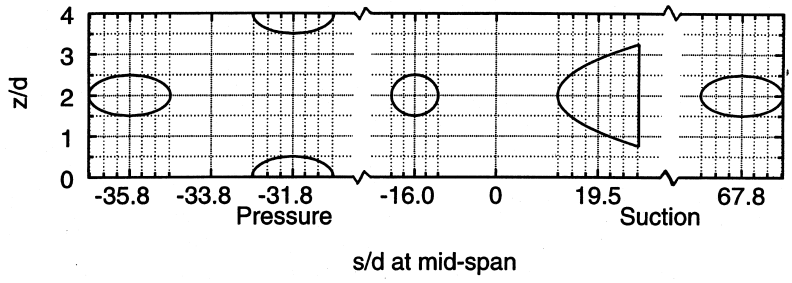

Fig. 2. Shape of film cooling holes at exit on the ACE rotor surface.

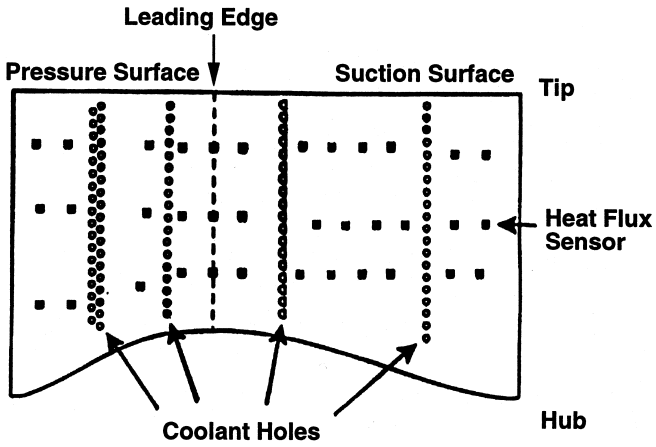

Fig. 3. Heat flux gauges and cooling hole locations on the projected blade surface with each of the three chordwise rows of gauges on a separate blade.

region is handled by imposing periodicity conditions across the airfoil. Figure 4 shows the grid on the rotor surface with suction surface in the front, and the C-grid on the hub. Only alternate grid lines are shown in this figure for the sake of clarity. Also, extension of the C-grid all the way to the shroud is not shown to avoid confusion. The location of the rows of holes is indicated by arrows. Computations were run on the 16-processor C90 supercomputer at the NASA Ames Research Center. For the two-equation turbulence model, the code requires about 182 million words (Mw) of storage and takes about 58 s per iteration (full-multigrid) on the C90 machine. For a given grid the first isothermal blade case requires about 1000 iterations to converge, while subsequent cases (corresponding to different values of the parameters) for the same grid require about 500 iterations starting with the solution for the previous case. While the iteration for solution proceeds through conservation of mass, momentum and energy for each control volume, the heat transfer coefficient at the blade surface was found to converge when the overall mass balance between the inlet and exit of the blade row was within 0.5%.

5. Results and discussion

The present numerical results were obtained by simulating the exact experimental conditions of the MIT experiment given in Table 1 for the cases compared. The blowing parameter, B_p, and the coolant temperature, T_c/T_o, at the hole exits were estimated from the static pressure distribution on an uncooled blade (found by executing the present code in the uncooled mode), and the relative total pressure and temperature measured in the coolant plenums, with coolant Mach number, relative to the rotor, restricted to unity at the hole-exit, assuming one-dimensional compressible flow through the hole-pipe. All holes in the second row (SS2) and most holes in the first row (SS1), especially those near the hub, on the suction surface were choked. Three film-cooled cases, Runs 71, 72 and 73, were selected for comparison, as detailed in Table 1. While case 71 represents near design-condition operation, test case 73 represents a lower pressure ratio and speed, and case 72 has a positive incidence angle. Figure 5 shows the variation of (isentropic) relative Mach number on the blade surface for the three

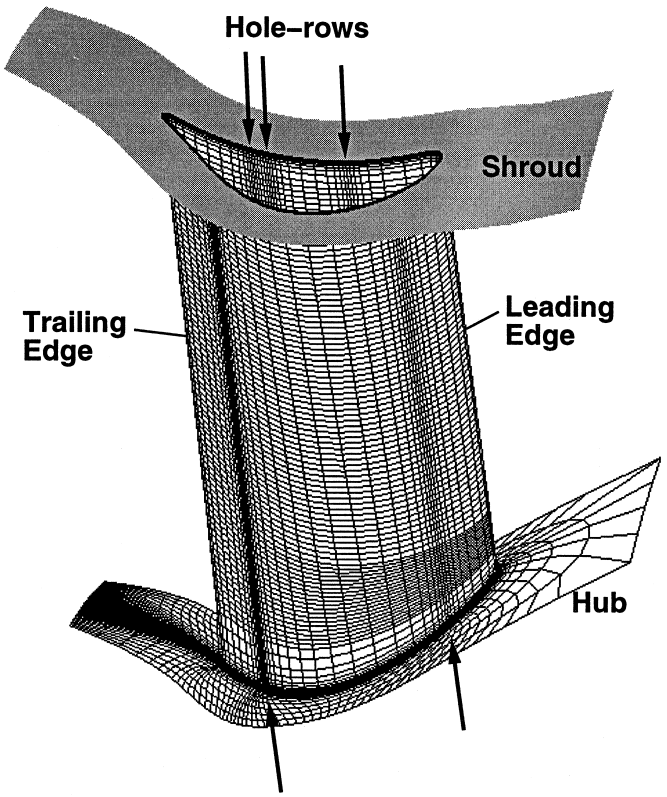

Fig. 4. Grid on the blade surface, and C-grid on the hub. Suction surface is in the front. Alternate grid lines shown.

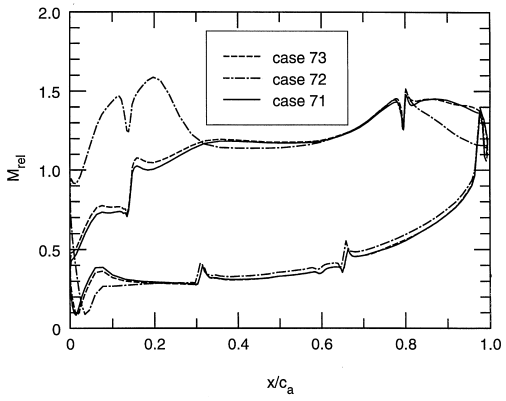

Fig. 5. Relative Mach number on the blade surface for various cases.

cases. While there is a little difference for cases 71 and 73, the effect of a positive incidence angle for case 72 is clearly visible on the suction surface. Except at the leading edge, the sudden changes in M_{rel} values occur at the locations of the film-cooling holes.

Figure 6 compares the predicted Nusselt number on the blade surface near the hub, mid-span and tip, computed using the k–ω, q–ω or Baldwin–Lomax model, with the experimental data for the film-cooled baseline case 71. The Nusselt number is based on the rotor axial chord, the relative total temperature at entry to the rotor, the blade temperature, and the gas thermal conductivity at the blade temperature. The abscissa is the fractional wetted pressure and suction surface of the blade. The five short vertical lines in this figure and in Figs 7 and 8 denote the location of film cooling rows. The experimental data are shown with error bars. Presence of negative values of Nu at some locations simply implies that the direction of heat transfer is reversed at these locations due to specification of the isothermal wall boundary condition and coolant temperature. The comparison is very good at the leading edge for the B–L model, generally good on the suction surface for all turbulence models but fairly poor downstream of PS1 on the pressure surface near the hub for the B–L and q–ω models. Only the k–ω model provides a good comparison with the experimental data on the pressure surface. It is interesting to note that near the hub section, where the best experimental data coverage is available, the suction surface heat transfer is very well

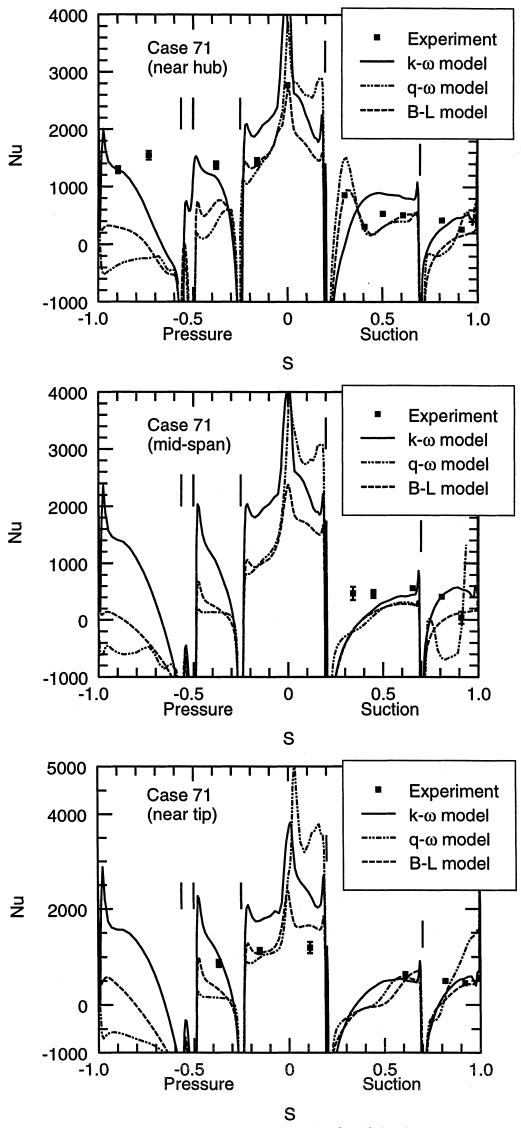

Fig. 6. Comparison of Nusselt number on the blade surface for case 71 near hub, mid-span and tip based on three turbulence models (near design-condition operation).

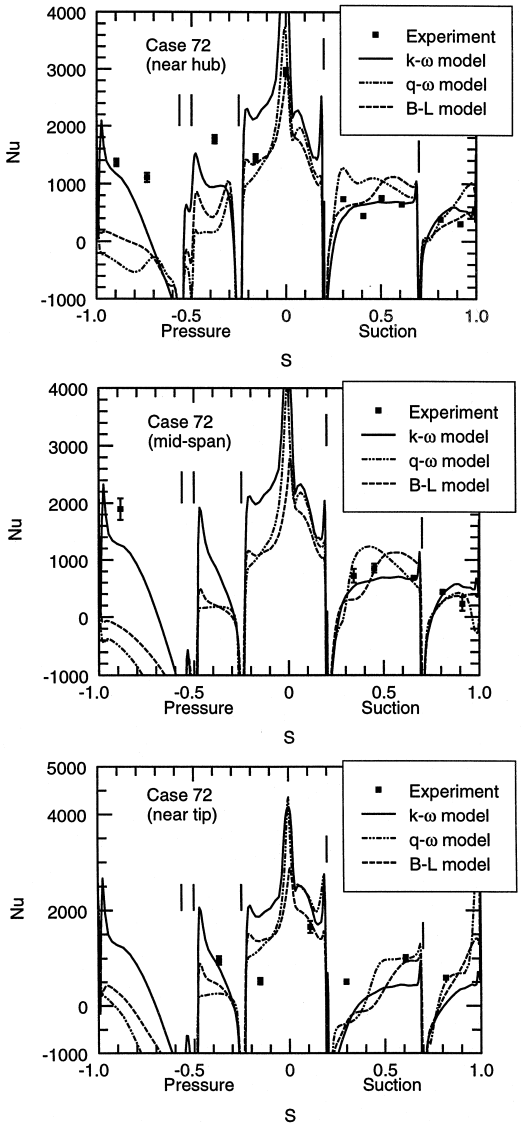

Fig. 7. Comparison of Nusselt number on the blade surface for case 72 near hub, mid-span and tip based on three turbulence models (positive incidence angle case).

predicted by all the models in terms of the level and the distribution of surface heat flux. On the pressure surface, however, both B–L and q–ω models under-predict the heat transfer considerably, while the k–ω model under-predicts it only a little. This comparison suggests that, in the presence of film cooling, all three turbulence models correctly simulate the driving mechanisms for heat transfer on the suction surface. On the pressure surface, however, only the k–ω model does a fair job.

In Figs 7 and 8, similar comparisons of numerical prediction of Nusselt number with the experimental data for film-cooled cases 72 and 73 are shown, respectively. It may be noted that Garg and Abhari [12] found similar under-prediction on the pressure surface and good comparison with experimental data on the suction surface for an uncooled case while using the B–L model. A possible cause for discrepancy in the comparison with the experimental data may be the result of uncertainty in the values of (a) the blowing parameter and coolant temperature which were estimated using the one-dimensional compressible flow through the hole-pipe, and (b) the relative flow angle at inlet to the rotor which was estimated from a through-flow streamline curvature calculation, in the

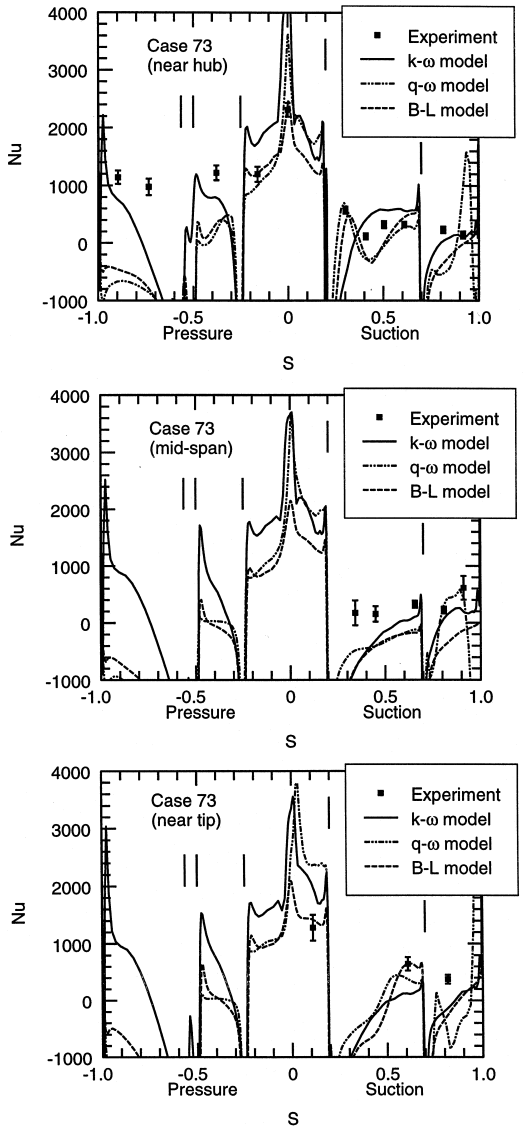

Fig. 8. Comparison of Nusselt number on the blade surface for case 73 near hub, mid-span and tip based on three turbulence models (lower speed and pressure ratio).

absence of experimental measurements. Also, the gas constant and specific heat ratios for the mainstream and coolant flow are different in the experiment owing to the use of different gas mixtures but the code assumes the same gas for both the main and coolant flows. Moreover, values of the discharge coefficients for the film-cooling holes were estimated, not measured. The blade surface was assumed to be isothermal while the experiment had 12–20% blade surface temperature variation. Finally, it is possible that the turbulent mixing on the low Mach number pressure surface is under-predicted by both the B–L and q–ω models. It may also be noted that the turbulence models were not modified to include any rotation effects. While the results in Figs 6–8 are based on a uniform coolant velocity and temperature distribution at the hole exits, specifying a polynomial distribution, like that in Garg and Gaugler [10], at the exit of the double-row of holes on the pressure surface, does not improve the comparison by more than 5% using the B–L model [12].

Figures 9–11 show Nusselt number contours at increments of 200 over the entire blade surface for the cases 71, 72 and 73, respectively, using the three turbulence models. Comparing the results for the three models for each case, we find that while the Nusselt number values on the pressure surface are nearly similar using the B–L and q–ω models but much higher using the k–ω model, those on the suction surface have large differences in the leading edge region, hub and tip regions, and near the trailing edge. The q–ω model results in much higher heat loads than the B–L model in these regions on the suction surface, while the k–ω model seems to predict heat loads between those of the B–L and q–ω models. Due to no film cooling over the leading edge portion, this part of the blade has a high Nusselt number for all models, being exposed to the hot stream for all the cases. Downstream of the first and subsequent rows of cooling holes on both the pressure and suction surfaces, the effect of film cooling is clearly evident as streaks of lower heat load and generally lower Nusselt number values. For the off-design case 72, the blade suction surface upstream of the second row of holes has higher Nusselt number values than the other two cases. On the other hand, case 73 has lower Nu values than all the other cases over almost the entire blade surface, and is thus the best-cooled case studied. It may also be observed that the Nusselt number is fairly high in the thick boundary layers on the suction surface near both the hub and the tip. From these figures, we observe that the Nusselt number is a strong function of the streamwise as well as the spanwise location, especially in the vicinity of film-cooling holes.

6. Conclusions

A comparison of blade surface heat transfer between a fully three-dimensional Navier–Stokes code with Wilcox's k–ω, Coakley's q–ω and Baldwin–Lomax turbulence models and the experimental data obtained on a transonic rotating rotor blade with film cooling is presented. All models provide a reasonably good prediction of the heat transfer on the suction surface of the film-cooled rotor blade when compared to the experimental data. At the leading edge, the Baldwin–Lomax model yields a much better comparison with the experimental value of Nusselt number than the k–ω or q–ω model. On the pressure surface, while k–ω provides a

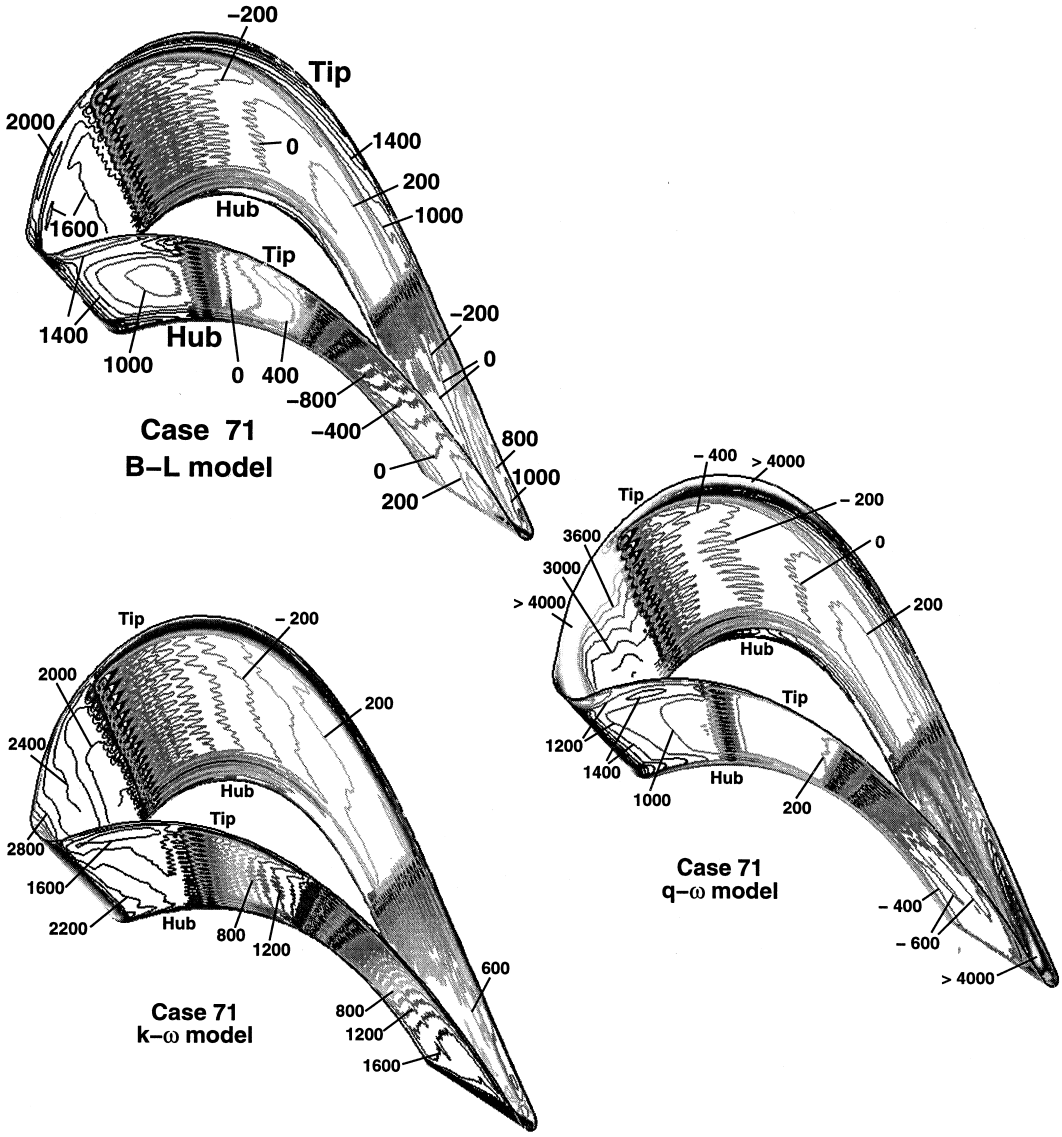

Fig. 9. Nusselt number contours on the ACE rotor for case 71 using three turbulence models (near design-condition operation).

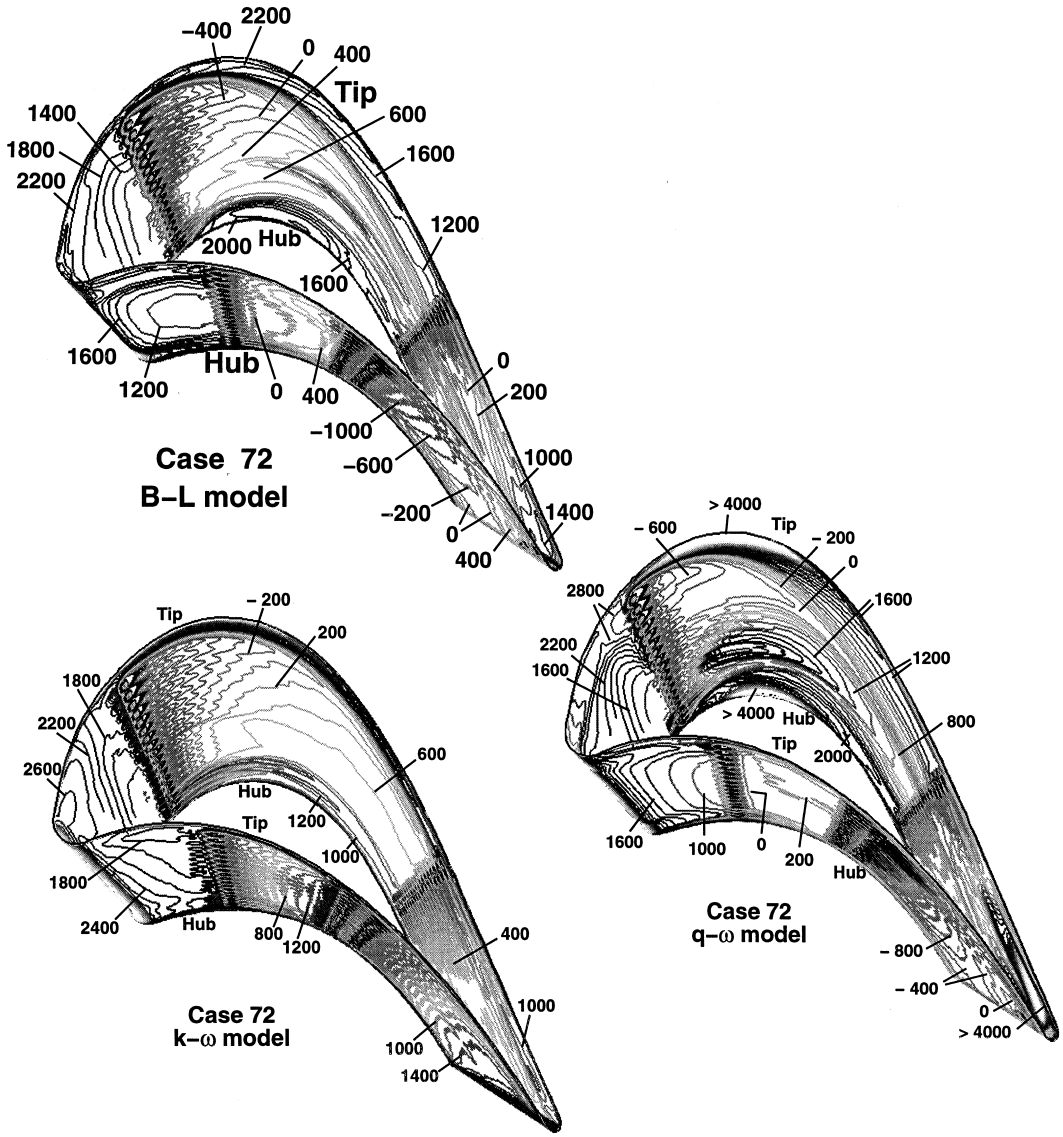

Fig. 10. Nusselt number contours on the ACE rotor for case 72 using three turbulence models (positive incidence angle case).

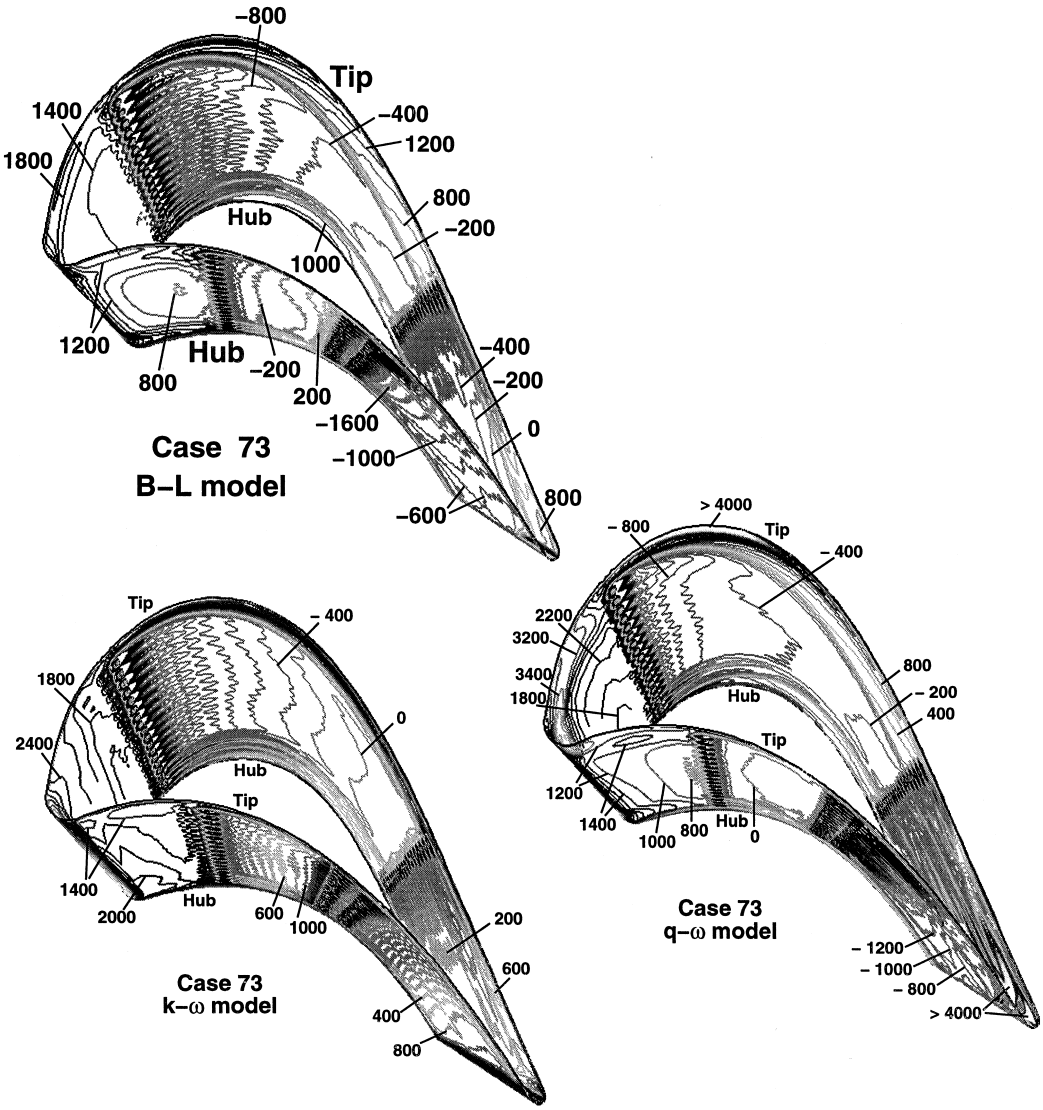

Fig. 11. Nusselt number contours on the ACE rotor for case 73 using three turbulence models (lower speed and pressure ratio).

much better comparison, both q–ω and B–L models under-predict the surface heat transfer considerably. The k–ω model does seem to provide the best overall comparison with the experimental data. However, a definite conclusion in this regard may await more experimental data on a film-cooled rotating blade. An overhead of some 40–50% in computational time and core requirement may also be noted while using a two-equation model rather than the B–L model.

Acknowledgements

The support provided by Dr Raymond Gaugler, Chief, Turbine Branch, and by Mr John Rohde of the Subsonic Systems Office at the NASA Lewis Research Center is gratefully acknowledged.

References

[1] R.J. Goldstein, Film cooling, in: T.F. Irvine, Jr., J.P. Hartnett (Eds.), Advances in Heat Transfer, vol. 7, Academic Press, New York, 1971, pp. 321–379.
[2] V.K. Garg, R.E. Gaugler, Heat transfer in film-cooled turbine blades, ASME Paper 93-GT-81, 1993.
[3] V.K. Garg, R.E. Gaugler, Prediction of film cooling on gas turbine airfoils, ASME Paper 94-GT-16, 1994.
[4] V.K. Garg, R.E. Gaugler, Leading-edge film-cooling effects

on turbine blade heat transfer. Numer. Heat Transfer, Part A 30 (1996) 165–187.
[5] M.E. Crawford, W.M. Kays, R.J. Moffat, Full coverage film cooling on flat, isothermal surfaces: A summary report on data and predictions, NASA CR 3219, 1980.
[6] B. Schönung, W. Rodi, Prediction of film cooling by a row of holes with a two-dimensional boundary-layer procedure. J. Turbomachinery 109 (1987) 579–587.
[7] D.K. Tafti, S. Yavuzkurt, Prediction of heat transfer characteristics for discrete hole film cooling for turbine blade applications, J. Turbomachinery 112 (1990) 504–511.
[8] R.S. Abhari, Impact of rotor–stator interaction on turbine blade film cooling, J. Turbomachinery 118 (1996) 123–133.
[9] V.K. Garg, R.E. Gaugler, Effect of coolant temperature and mass flow on film cooling of turbine blades, Int. J. Heat Mass Transfer 40 (1997) 435–445.
[10] V.K. Garg, R.E. Gaugler, Effect of velocity and temperature distribution at the hole exit on film cooling of turbine blades, J. Turbomachinery 119 (1997) 343–351.
[11] V.K. Garg, Adiabatic effectiveness and heat transfer coefficient on a film-cooled rotating blade, Numer. Heat Transfer, Part A 32 (1997) 811–830.
[12] V.K. Garg, R.S. Abhari, Comparison of predicted and experimental Nusselt number for a film-cooled rotating blade, Int. J. Heat and Fluid Flow 18 (1997) 452–460.
[13] V.K. Garg, A.A. Ameri, Comparison of two-equation turbulence models for prediction of heat transfer on film-cooled turbine blades, Numer. Heat Transfer, Part A 32 (1997) 347–371.
[14] D. Choi, A Navier–Stokes analysis of film cooling in a turbine blade, AIAA Paper 93-0158, 1993.
[15] R.P. Dring, M.F. Blair, H.D. Joslyn, An experimental investigation of film cooling on a turbine rotor blade, J. Engg. for Power 102 (1980) 81–87.
[16] R.S. Abhari, An experimental study of the unsteady heat transfer process in a film cooled fully scaled transonic turbine stage, Ph.D. thesis, Massachusetts Institute of Technology, 1991.
[17] K. Takeishi, S. Aoki, T. Sato, K. Tsukagoshi, Film cooling on a gas turbine rotor blade, ASME Paper 91-GT-291, 1991.
[18] A. Arnone, Viscous analysis of three-dimensional rotor flow using a multigrid method, J. Turbomachinery 116 (1994) 435–445.
[19] H. Schlichting, Boundary Layer Theory, 7th ed., McGraw-Hill, New York, 1979, p. 328.
[20] A. Jameson, W. Schmidt, E. Turkel, Numerical solutions of the Euler equations by finite volume methods using Runge–Kutta time-stepping schemes, AIAA Paper 81-1259, 1981.
[21] A. Brandt, Multi-level adaptive computations in fluid dynamics, AIAA Paper 79-1455, 1979.
[22] A. Jameson, Transonic flow calculations, MAE Report 1651, MAE Department, Princeton University, 1983.
[23] L. Martinelli, Calculations of viscous flows with a multigrid method, Ph.D. thesis, Princeton University, 1987.
[24] B.S. Baldwin, H. Lomax, Thin-layer approximation and algebraic model for separated turbulent flows, AIAA Paper 78-257, 1978.
[25] T.J. Coakley, Turbulence modeling methods for the compressible Navier–Stokes equations, AIAA Paper 83-1693, 1983.
[26] F.R. Menter, Zonal two equation k–ω turbulence models for aerodynamic flows, AIAA Paper 93-2906, 1993.
[27] D.C. Wilcox, Simulation of transition with a two-equation turbulence model, AIAA J. 32 (1994) 247–255.
[28] A.A. Ameri, A. Arnone, Navier–Stokes turbine heat transfer predictions using two-equation turbulence closures, AIAA Paper 92-3067, 1992.
[29] A.A. Ameri, A. Arnone, Prediction of turbine blade passage heat transfer using a zero and a two-equation turbulence model, ASME Paper 94-GT-122, 1994.
[30] R.V. Chima, A k–ω turbulence model for quasi-three-dimensional turbomachinery flows, AIAA Paper 96-0248, 1996.
[31] R.J. Boyle, P. Giel, Three-dimensional Navier–Stokes heat transfer predictions for turbine blade rows, AIAA Paper 92-3068, 1992.
[32] E.J. Hall, D.A. Topp, R.A. Delaney, Aerodynamic heat transfer analysis of discrete site film-cooled turbine airfoils, AIAA Paper 94-3070, 1994.